• Intelligent Ophthalmology •

Automatic fovea detection and choroid segmentation for choroidal thickness assessment in optical coherence tomography

Chen Yu Lin[1], Hung Ju Chen[1], Yi Kit Chan[2], Wei Ping Hsia[1], Yu Len Huang[2], Chia Jen Chang[1]

[1]Department of Ophthalmology, Taichung Veterans General Hospital, Taichung 407, Taiwan, China
[2]Department of Computer Science, Tunghai University, Taichung 407, Taiwan, China
Correspondence to: Chia Jen Chang. No.1650, Sec. 4, Taiwan Blvd., Xitun Dist., Taichung 407, Taiwan, China. capmchangcj@gmail.com; Yu Len Huang. No.1727, Sec. 4, Taiwan Blvd., Xitun Dist., Taichung, 407, Taiwan, China. yihuang@thu.edu.tw
Received: 2023-10-04   Accepted: 2024-06-06

Abstract
● **AIM:** To develop an automated model for subfoveal choroidal thickness (SFCT) detection in optical coherence tomography (OCT) images, addressing manual fovea location and choroidal contour challenges.

● **METHODS:** Two procedures were proposed: defining the fovea and segmenting the choroid. Fovea localization from B-scan OCT image sequence with three-dimensional reconstruction (LocBscan-3D) predicted fovea location using central foveal depression features, and fovea localization from two-dimensional en-face OCT (LocEN-2D) used a mask region-based convolutional neural network (Mask R-CNN) model for optic disc detection, and determined the fovea location based on optic disc relative position. Choroid segmentation also employed Mask R-CNN.

● **RESULTS:** For 53 eyes in 28 healthy subjects, LocBscan-3D's mean difference between manual and predicted fovea locations was 170.0 μm, LocEN-2D yielded 675.9 μm. LocEN-2D performed better in non-high myopia group (*P*=0.02). SFCT measurements from Mask R-CNN aligned with manual values.

● **CONCLUSION:** Our models accurately predict SFCT in OCT images. LocBscan-3D excels in precise fovea localization even with high myopia. LocEN-2D shows high detection rates but lower accuracy especially in the high myopia group. Combining both models offers a robust SFCT assessment approach, promising efficiency and accuracy for large-scale studies and clinical use.

INTRODUCTION

The choroid, among tissues with the highest metabolic rate in the body, is located between the retina and the sclera. It supplies oxygen and metabolic needs to the retina, and is indispensable for the visual function[1]. The choroid is composed of three layers with different vessel sizes and physiology: the choriocapillaris, Sattler's layer, and Haller's layer[2].

With the development of optical coherence tomography (OCT), structures of the posterior visual segment such as the retinal and choroidal layers can be discriminated and measured. By depicting and measuring the thickness of choroidal layers in OCT images, features and their subtle details can be evaluated in some ocular diseases. Changes in thickness of choroid with age and ocular diseases have been reported[3-4]. Previous studies showed a negative correlation between choroidal thickness and age in the healthy population[5-6]. On the other hand, choroidal thickness and morphology are influenced not only by physiological factors such as age, refractive error, and axial length, but also in pathological conditions such as age-related macular degeneration, polypoidal choroidal vasculopathy, chorioretinitis, and autoimmune diseases[7-9]. Furthermore, systemic diseases such as diabetes, hypertension, and multiple sclerosis are known to be associated with changes in choroidal thickness. Notably, such alterations in the choroid may manifest even before the onset of retinopathy or systemic disorders[10-13].

Several approaches have been reported to evaluate choroidal thickness, including specific location and general assessments. The former involves subfoveal choroidal thickness (SFCT),

at sites located at certain distance (*e.g.*, 1 or 3 mm) from the fovea in the temporal, nasal, superior or inferior directions[14-16]; and the latter involves continuous calculation for intact evaluation[17-19]. In most instances, the choroid underneath the central macular region, also known as SFCT, presents the maximal thickness compared with other choroid sites. SFCT is widely regarded as a valuable and significant indicator in assessing choroidal status, such as pathological changes in choroid, changes in thickness with aging and refraction status, and even in its correlation with cardiovascular diseases[7,20].

Since manually both locating the fovea and outlining the contours of the choroid are inconvenient and time-consuming for large-scale investigation. Additionally, achieving reliable repeatability in manual sketching is difficult to achieve due to the ambiguous border of the choroid. Therefore, a reliable technique with automatic detection of SFCT can ameliorate the above predicament and evaluate SFCT more effectively and accurately. Based on above statement, an automatic model for SFCT detection is practical and important.

To measure SCFT automatically, there are two crucial procedures: 1) defining the location of the fovea, 2) segmenting the choroid. Several recent studies have advanced automatic choroid detection methodologies. Li *et al*[21] employed a group-wise context selection network in conjunction with swept-source OCT to identify the choroid in highly myopic individuals. Yan *et al*[22] introduced a context-efficient adaptive network for choroid thickness computation, yielding satisfactory outcomes in healthy subjects. Masood *et al*[23] proposed a model that integrates convolutional neural networks (CNNs) with morphological techniques to extract only superficial features. Hsia *et al*[24] introduced the mask region-based CNN (Mask R-CNN), which has demonstrated the ability to retain critical information and features. When applied to choroidal segmentation, it achieves automatic, precise, and efficient prediction of choroidal boundaries. Subsequent studies utilizing Mask R-CNN have confirmed its robustness and reliability in various conditions[5,25]. In this study, we specifically apply the Mask R-CNN model for choroid segmentation.

In automatic fovea detection, a precise understanding of the macular contour is crucial. The anatomical definition of the fovea describes it as a depression at the center of the macula. OCT images offer detailed anatomical insights and come with benefits such as rapid examination and not requiring pupil dilation. Therefore, we designed our fovea detection model in this study using OCT images[26-27]. Our approach involves a 3-dimensional (3D) reconstruction model to automatically identify the anatomical depression in OCT sequences, adhering closely to the anatomic definition, and complemented by a 2-dimensional (2D) model to enhance comprehensiveness.

In our study, we aimed to develop a reliable model for predicting SFCT automatically. In choroidal segmentation, the proposed Mask R-CNN model was applied. Regarding fovea detection, a novel model comprising 3D reconstruction of OCT sequences and complementary 2D information was introduced and validated.

SUBJECTS AND METHODS

Ethical Approval This study adhered to the principle of the Declaration of Helsinki and was approved by the Institutional Review Board of Taichung Veterans General Hospital, Taiwan, China (approval number: CE21201B), with an exemption granted for informed consent.

Participants and Data Acquisition We recruited participants over 18 years of age and had no significant ocular diseases from Taichung Veterans General Hospital, Taiwan. We excluded participants who had a history of intraocular intervention or significant ocular diseases that could potentially impact the retina and choroid, such as ocular tumor, diabetic retinopathy, inflammatory diseases, age-related macular degeneration, or subretinal fluid. However, we did not exclude those with high myopia, defined as a spherical equivalent <-6.0 diopter (D). This criterion was made to investigate the detection ability of our model and to gather more information from this specific population. In total, we included 53 eyes from 28 healthy subjects for our study.

All participants underwent a spectral domain OCT scan with enhanced depth imaging mode (Heidelberg Engineering, Heidelberg, Germany). The scan images provided adequate quality and depth for the evaluation of choroidal layers. Each OCT scan sequence consisted of 97 2D slices covering an area of 6 mm×6 mm centering at the fovea. En-face OCT was also recorded. The fovea location for each OCT sequence was identified first by ophthalmologists, and the choroid boundary on the corresponding slice. The boundary results were carefully confirmed by two ophthalmologists.

Image Instances Segmentation-Mask R-CNN The Mask R-CNN model has a two-stage framework[28]. In the first stage, the input images were convolved to produce distinctive feature maps and proposals through a regional proposal network (RPN). The RPN utilizes the backbone network (typically either ResNet-50 or ResNet-101; in our study, we used the ResNet-50) to generate the feature maps from the input images. These features are then passed onto the RPN to generate proposals for the coordinates of the optic disc. In the second stage, the proposals were classified by a fully convolutional network (FCN) to generate bounding boxes and masks, and the final feature maps were finally produced. The Mask R-CNN approach was deployed to delineate the desired regions in this study.

To assess the robustness of the models across varying image conditions, we employed K-fold cross-validation on the

dataset. K-fold cross-validation is a technique used to evaluate model performance, ensuring validity across the dataset without bias towards specific images and guarding against overfitting. Widely utilized in the realm of machine learning, it examines whether model performance remains consistent both within and beyond the dataset. In this study, we implemented 5-fold cross-validation. The dataset was randomly divided into 5 equal groups, and training was conducted 5 times. During each training iteration, 4 groups served as the training set, while the remaining group served as the testing set. This process was repeated until all groups had been trained and tested, with the results being averaged across all folds to determine overall performance.

Automatic Fovea Detection　Figure 1 showed the flowchart of the proposed method for choroidal thickness assessment. Two models for automatic fovea detection were proposed in this study, namely 1) the fovea localization from the B-scan OCT image sequences with 3D reconstruction (LocBscan-3D), and 2) fovea localization from 2D en-face OCT images (LocEN-2D). By the combined strengths of these two models, we aimed to provide the comprehensive and accurate fovea prediction. Details of these two models are explained below.

LocBscan-3D　For data preprocessing, we expanded the coordinates to create a shape suitable for our model to construct a series of 3D images. In image processing, linear interpolation is commonly used for tasks such as image resizing or resampling. Linear interpolation provides a simple method for estimating the gray-level values of these new pixels based on the gray-level of nearby pixels. The linear interpolation algorithm was hence used to expand each image 5 times the original 2D OCT images with 97 slices per sequence, resulting in a new series of images. Figure 2 illustrated the construction of the LocBscan-3D model.

In the 3D reconstructed image, our model scanned from the innermost portion of the retina and progressed slice by slice towards the outermost area of the sclera. The vitreous cavity appeared to be non-reflective or hyporeflective at first, turning to hyperreflective until the scanned area had reached the inner limiting membrane. Given the characteristic of central depression of the fovea, we defined the fovea location at the point where the non-reflective area disappeared, up to the last detectable slice of the model. In this study, we utilized the Mask R-CNN model to isolate the non-reflective region within each 3D reconstructed image.

To predict the fovea location from the 3D images, we applied linear prediction to extract the result and identified the vanishing point. The vanishing point represents the critical coordinates revealing the fovea location, and the smallest vanishing point was considered as the fovea location in the
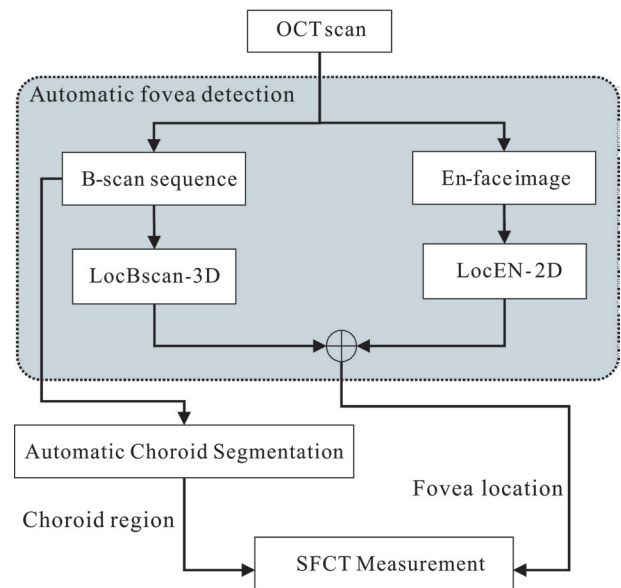
Figure 1 Flowchart of the proposed method　Two models were designed for automated fovea detection: LocBscan-3D and LocEN-2D. Furthermore, the integration of automatic choroid segmentation enabled the derivation of SFCT. LocBscan-3D: Fovea localization from B-scan OCT image sequence with three-dimensional reconstruction; LocEN-2D: Fovea localization from two-dimensional en-face OCT image; SFCT: Subfoveal choroidal thickness; OCT: Optical coherence tomography.
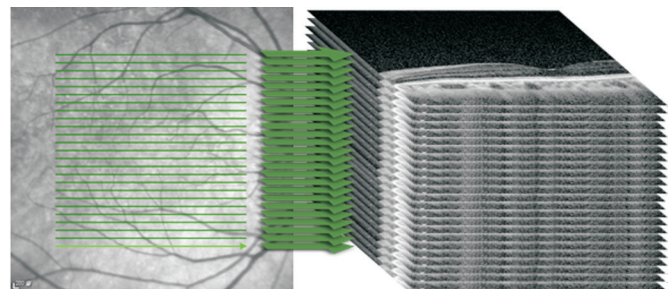
Figure 2 Depiction of LocBscan-3D model (simplified)　Each OCT sequence with 97 2D slices were expanded five times by interpolation algorithm, and the 3D image collection was constructed subsequently. LocBscan-3D: Fovea localization from B-scan OCT image sequence with three-dimensional reconstruction; OCT: Optical coherence tomography.

image. Figure 3 showed an example of the predicted fovea location with the LocBscan-3D model. Since images had been artificially expanded, we used a reverse interpolation after extracting the results to transform them back to 2D images of the original size. The process enabled accurate matching of the slices and calculation of the proper slice coordinates.

LocEN-2D　This study also utilized the Mask R-CNN model to delineate the optic disc area from the en-face OCT images. After identifying the optic disc, we defined the fovea location in this model as 4.5 mm temporal and 0.65 mm inferior to the center of the optic disc. This determination was based on the findings reported in previous publications[27-29]. We then

Table 1 The mean distances between the fovea locations labeled by ophthalmologists and those predicted by the automatic prediction model   mean±SD

Predicted models	x-axis (pixels)	y-axis (pixels)	z-axis (slices)	Overall distance[a] (μm)
LocBscan-3D (*n*=51)	12.8±3.7	7.7±1.3	0.7±0.7	170.0±43.0[b]
LocEN-2D (*n*=53)	46.8±44.1	34.4±28.8	2.0±3.8	675.9±500.0[b]

LocBscan-3D: Fovea localization from B-scan OCT image sequence with three-dimensional reconstruction; LocEN-2D: Fovea localization from two-dimensional en-face OCT image; SD: Standard deviation. [a]According to the machine's settings, each pixel or slice in the x-, y-, and z-axes corresponds to 12, 4, and 66 μm, respectively. After converting pixels to lengths in each axis, the distance between manual depiction and automatic detection was calculated accordingly. The overall distance represents the of each case. [b]*P*<0.01 for the mean distance between the two models.

transferred the fovea location from the en-face OCT to the corresponding coordinates on the B-scan slices.

**Automatic Choroid Segmentation and SFCT Measurement** In our study, we evaluated SFCT using several methods, including manual delineation by ophthalmologists and prediction from the Mask R-CNN model. The Mask R-CNN model was used for choroid segmentation as well[24]. SFCT was calculated vertically from the inner boundary of the choroid to the outer boundary underneath the predicted fovea. SFCT measurements were obtained by combining the choroid area predicted by the Mask R-CNN model and the fovea location labeled by ophthalmologists and later identified using the LocBscan-3D and LocEN-2D models as mentioned above.

Statistical Analysis Fovea locations on OCT images predicted by the LocBscan-3D model, LocEN-2D model, and labeled by ophthalmologists were expressed in a coordinate system. The distances between the fovea locations defined manually and the two automatic prediction models were calculated and compared. SFCT was also measured based on the fovea location predicted by the LocBscan-3D and LocEN-2D models.

Subjects with and without high myopia were further analyzed. A paired *t*-test was performed to compare the difference in predictive accuracy between two models. A two-sample *t*-test was applied to compare the differences between groups regarding myopic condition and SFCT prediction. Linear regression and Spearman's correlation were used to examine the relationship between refractive error and foveal detection accuracy. Statistical analyses were performed using SPSS (version 20). Data were presented as mean±standard deviation. Statistical significance was set at a two-tailed *P*<0.05 for all statistical analyses.

RESULTS

In this study, a total of 53 eyes from participants without significant ocular diseases were analyzed. Among them, 25 were right eyes and 28 were left eyes. The mean age of participants was 40.1±10.5 years old. Their average spherical equivalent was -5.0±2.84 D, with -3.09±1.46 D in the non-high myopia group (*n*=33) and -8.28±1.20 D in the high myopia
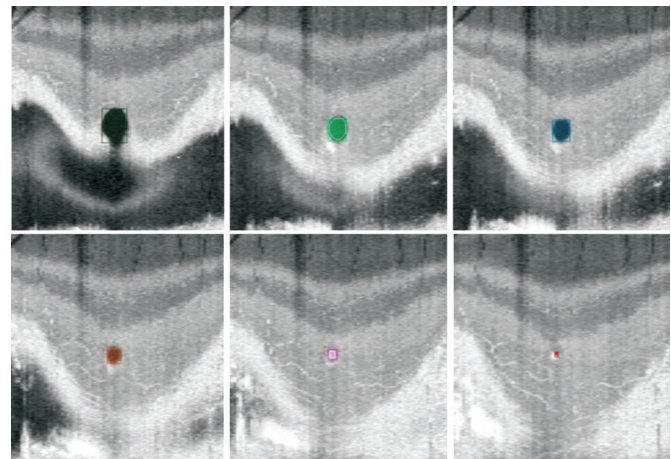
Figure 3 Illustration of a case using LocBscan-3D model The model utilize the scan from the innermost portion of the retina and progressed slice by slice towards the outer portion in order to detect the fovea location. As the scan went deeper, the round non-reflective area (colored in the figure) became progressively smaller. The fovea location was defined as the point at which the non-reflective area disappeared, which was detected in the last slice by the model. LocBscan-3D: Fovea localization from B-scan OCT image sequence with three-dimensional reconstruction; OCT: Optical coherence tomography.

group (*n*=20). Each OCT sequence was processed with both the LocBscan-3D and LocEN-2D model, and fovea locations were automatically predicted. Subsequently, SFCT were calculated by the Mask R-CNN model.

Figure 4 illustrated an example of fovea locations as identified by different methods. Fovea locations were recorded in a coordinate system with x and y axes and different OCT slices. Table 1 showed the mean distances between the manually identified fovea locations and those predicted by models. Totally 51 out of 53 OCT sequences were successfully processed by the LocBscan-3D model, with fovea locations automatically identified. The mean differences from the ophthalmologists' manually identified values and predicted values of the LocBscan-3D model were 12.8 pixels in the x-axis, 7.7 pixels in the y-axis, and 0.7 slices (considered as the z-axis) as shown in the OCT scan. According to the

Table 2 Comparison of non-high myopia group and high myopia group

| Predicted models	Non-high myopia	High myopia
LocBscan-3D		
No. of eyes	33	20
Mean SE (diopter)	-3.86±1.16	-8.28±1.20
Distance[a] (μm)	169.1±41.6	171.5±45.0
P[b]	0.85	
LocEN-2D		
No. eyes	31	20
Mean SE (diopter)	-3.09±1.46	-8.28±1.20
Distance[a] (μm)	529.9±345.0	916.9±608.5
P[b]	0.02	

SE: Spherical equivalents; LocBscan-3D: Fovea localization from B-scan OCT image sequence with three-dimensional reconstruction; LocEN-2D: Fovea localization from two-dimensional en-face OCT image; OCT: Optical coherence tomography. [a]The distances between the fovea locations labeled by ophthalmologists and those predicted by the automatic prediction model. [b]Comparison of the distances between the results from the non-high myopia group and the high myopia group.

machine's settings, each pixel or slice in the x-, y-, and z-axes corresponds to 12, 4, and 66 μm, respectively. After converting pixels to distance values, the overall distance was 170.0 μm. In addition, all 53 OCT sequences were processed successfully by the LocEN-2D model, and foveal locations were detected. The mean discrepancies between the foveal locations predicted by the LocEN-2D model and those identified by ophthalmologists were 46.8 pixels in the x-axis, 34.4 pixels in the y-axis, and 2.0 slices in the OCT scan (considered as the z-axis). The overall distance was 675.9 μm after converting pixels to the corresponding distance values. A significant difference between the two models was observed ($P<0.01$).

When subjects were categorized into non-high myopia and high myopia groups, Table 2 displayed the discrepancies between manually identified foveal locations and those predicted by automatic models. The LocEN-2D model exhibited poorer predictive accuracy in the high myopia group (529.8 μm in the non-high myopia group and 916.0 μm in the high myopia group, $P=0.02$), whereas the LocBscan-3D model revealed similar predictive results between the two groups (169.1 μm in the non-high myopia group and 171.5 μm in the high myopia group, $P=0.85$). A regression model was conducted to investigate the relationship between myopic refraction error and the discrepancies between manually identified and model-predicted locations. Figure 5A presents the results of the LocEN-2D model ($R^2=0.2291$), while Figure 5B displays the results of the LocBscan-3D model ($R^2=0.0017$). The LocBscan-3D model exhibited steady predictive results, unaffected by differences in refractive status.
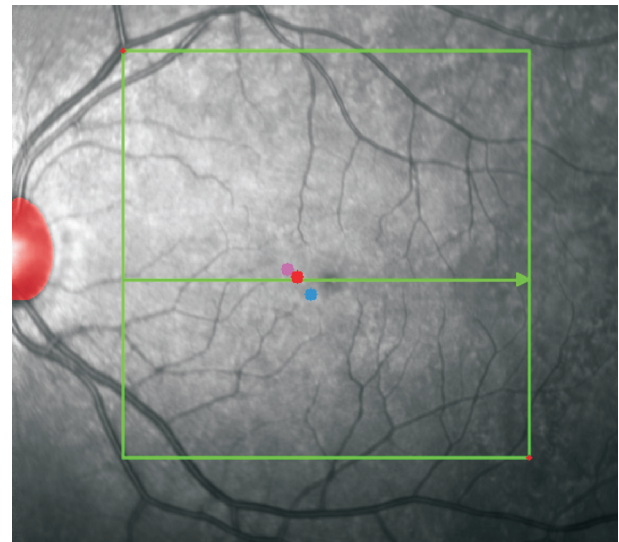
Figure 4 The different methods used to define the fovea location The fovea site labelled by ophthalmologist is represents by the red point, the blue point represents the fovea location predicted by LocEN-2D model, and the pink point represents the fovea location predicted by LocBscan-3D model. The red shaded area represents the position of the optic disc detected by the Mask R-CNN model. The green arrow indicates the OCT slice in which the ophthalmologist labeled the fovea. LocBscan-3D: Fovea localization from B-scan OCT image sequence with three-dimensional reconstruction; LocEN-2D: Fovea localization from two-dimensional en-face OCT image; OCT: Optical coherence tomography; Mask R-CNN: Mask region-based convolutional neural network.
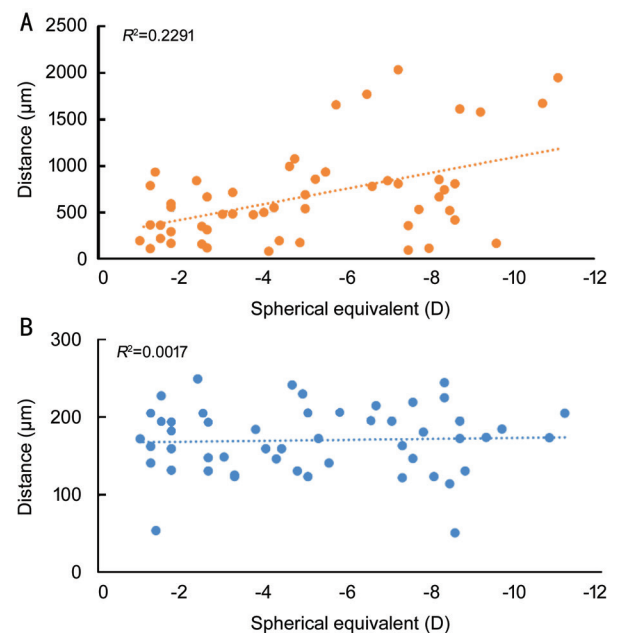
Figure 5 The relationship between myopic refraction error and the discrepancies between manually identified and model-predicted locations A: The result of LocEN-2D model; B: The result of LobBscan-3D model. LocBscan-3D: Fovea localization from B-scan OCT image sequence with three-dimensional reconstruction; LocEN-2D: Fovea localization from two-dimensional en-face OCT image; OCT: Optical coherence tomography.

Table 3 SFCT measured by different methods

Items	Predicted models[a]			Reference[b]
Identification of fovea locations	Manually[c]	LocBscan-3D	LocEN-2D	Manually[c]
SFCT (μm)	207.8±47.4	206.8±43.4	205.3±43.8	216.8±48.8
P[d]	0.35	0.49	0.23	-

SFCT: Subfoveal choroidal thickness; LocBscan-3D: Fovea localization from B-scan OCT image sequence with three-dimensional reconstruction; LocEN-2D: Fovea localization from two-dimensional en-face OCT image. [a]The choroidal boundary and thickness were detected using a mask region-based convolutional neural network model; [b]The choroidal boundary and thickness were delineated by ophthalmologists; [c]The foveal locations were identified by ophthalmologists; [d]Comparison with reference data.

Table 3 showed SFCT measurements obtained both from the predicted models generated by the Mask R-CNN model and manual delineation by physicians. The mean SFCT labeled by physicians was 216.8±48.8 μm, with no significant differences observed in SFCT predicted by the Mask R-CNN model across various foveal locations identified by different methods [206.8±43.4 μm (P=0.49) for foveae predicted by LocBscan-3D model, 205.3±43.8 μm (P=0.23) for foveae predicted by LocEN-2D model and 207.8±47.4 μm (P=0.35) for foveae labeled by physicians].

DISCUSSION

Our principal findings of this study are the following: 1) LocBscan-3D model predicted the foveal location accurately, regardless of high myopia or not; 2) LocEN-2D model exhibited a high detection rate for locating the optic disc and fovea, although it demonstrated lower accuracy, especially in high myopia; 3) Combining the Mask R-CNN model for choroid detection and automatic foveal detection model together, comprehensive and precise predict SFCT in the OCT images was demonstrated.

In our study, the LocBscan-3D model successfully analyzed around 96% of the OCT sequences (51 out of 53 cases). Regarding the two cases that failed to be analyzed, the reason is likely due to oblique and not flat macula in the OCT scans. On the other hand, using the LocEN-2D model, although the accuracy of prediction in foveal location was lower than LocBscan-3D, all 53 cases were processed because of the qualified and comprehensive predictions observed in the Mask R-CNN model for optic disc detection. This allowed for the subsequent prediction of the corresponding foveal center position. Although there were slight discrepancies in foveal position between manual labeling and predictions by either the LocBscan-3D model or the LocEN-2D model, the predicted SFCT did not exhibit significant differences. This could be explained by the fact that the choroid contour tends to be relatively continuous and smooth. Therefore, the overall smoothness of the choroid contour may mitigate the impact of less precise foveal localization on SFCT measurements.

The automatic detection model for the fovea and SFCT in our study is robust and has the potential to be applied in large-scale population screening. Changes in choroidal thickness are related to systemic diseases. For example, a significant decrease in choroidal thickness is known to precede clinical symptoms in diabetic retinopathy[30-31]. Early complications of hypertension are also detected by changes in choroidal thickness[10,32-33]. By utilizing the model to detect changes in choroid thickness, clinicians may be able to identify subtle changes in ocular health and to more effectively monitor disease progress, leading to better management strategies, providing prompt intervention and probably improving clinical outcomes.

To develop an automatic detection model for the SFCT, ideal fovea identification is the first and foremost task, followed by precise segmentation of the choroidal layer. Several studies have described methods on automatic detection of the fovea. Liefers et al[34] trained a CNN model for fovea detection based on a set of 781 OCT scans, and reported a detection rate of around 96%, which is comparable to the performance of our models. Hussain et al[35] described a standard deviation profiling method that had extracted features from the inner limiting membrane, and the fovea was detected subsequently using a rule-based approach, but with difficulty in dealing with non-intact foveal layer. Limitations of these previous studies included that limited conditions were confined in the training model, and some methods were unable to organize information across multiple B-scans. By constructing a 3D-structure map from multiple B-scans in OCT imaging, the fovea location can be identified more intuitively. This allows for the detection of the small central depression, known as the anatomical definition of the fovea. Consequently, our LocBscan-3D model accurately predicted the fovea location in individuals with a healthy macula. Thus, our method demonstrated reliable and precise results for automatic fovea detection.

Regarding choroid layer detection, various studies have been mentioned in the introduction section. Previous research employing Mask R-CNN has demonstrated a dice similarity coefficient (DSC) of approximately 95% between automatically and manually segmented regions, with an average error ranging from 4 to 5 pixels. In comparison, the group-wise context selection network by Li et al[21] achieved

a DSC of around 93%, requiring swept-source OCT, which is less commonly available for screening purposes. Additionally, compared to models introduced by Yan et al[22], the average error ranged from 4 to 12 pixels. Another widely used neural network for medical image segmentation, the U-shape convolutional network, reported a predictive error of 21.84 μm with a DSC of 92.8%. However, it didn't yield superior results compared to Mask R-CNN, which achieved a DSC of around 95% with an error of 13.75 μm in a previous study and less than 10 μm in the current study. Considering the above statements, the application of Mask R-CNN for choroid segmentation appears to be optimal.

Relevant 3D reconstruction techniques have been reported. Xu et al[36] utilized deep CNN and 3D morphometry to differentiate between normal retina, subretinal fluid, and cystoid macular edema. The results showed that the DSC of segmentation reached 0.78 for cystoid macular edema, 0.82 for subretinal fluid, and 0.95 for retina segmentation. Huang et al[37] compared the 3D choroidal vascularity index between fellow eyes of angle-closure glaucoma and the eyes of normal controls, which showed slightly higher index and thickness in the fellow eye of glaucoma. In comparison with our study, choroid segmentation was not performed in Xu et al's[36] publication, and there was no comparable manually labeled reference in Huang et al's[37] report. Hence, our model, which combines 3D reconstruction in the retina and Mask R-CNN for choroid detection, still retains novelty and significance.

The LocBscan-3D model may encounter difficulty in detecting the fovea in cases where contour of the central depression is obscure. This could be due to conditions such as center-involved macular edema, scarring, epiretinal membrane leading to traction, or presence of a non-flat macula, including posterior staphyloma or other situations involving a tilted macula. In order to overcome this challenge, the alternative approach of using a LocEN-2D model can be employed for the ability of comprehensive detection. The LocEN-2D model can provide acceptable results and can serve as a fallback option when the LocBscan-3D model fails to detect the fovea in a minority of cases. As the Mask R-CNN model can successfully predict the optic disc in almost 100% of cases, a mathematical method based on distance can be used to determine the fovea location. By combining these two models, strengths of each model can be leveraged. For example, priority should be given to utilizing the LocBscan-3D model, taking advantage of its accurate predictions of both fovea and SFCT. When the LocBscan-3D model fails to detect the fovea, possibly due to factors such as an obscured central depression contour, the LocEN-2D model can be employed as an alternative solution. While the LocEN-2D model may not provide fovea predictions as precise as desired, the discrepancies in SFCT predictions are negligible.

Furthermore, it consistently locates the fovea, rendering it a reliable fallback option. By harnessing the strengths of both models, comprehensive SFCT detection can be achieved. In determining the relative position between the optic disc and fovea, we incorporated findings from several previous studies. The American Academy of Ophthalmology[27] and Orth et al[38] reported that the fovea was located approximately 4.0 mm temporally and 0.8 mm inferiorly from the center of the optic disc. Williams and Wilkinson[28] reported approximately 4.91 mm being the average distance from the optic nerve head to the fovea center. Klaus reported a mean angle between the center of the fovea and the optic disc from the horizon of -5.6 degrees[29]. After incorporating the above findings, our LocEN-2D model considered the relative distance from the optic disc and used that to determine the fovea location.

The LocBscan-3D model utilizes the anatomical definition and features of the foveal depression, allowing for accurate fovea prediction. On the other hand, the LocEN-2D model exhibits larger prediction deviations and variations, particularly in cases with high myopia. By reviewing previous publications, variations in the relative position between the optic disc and fovea exist across reported studies[28-29,39-41]. Significant inter-individual variations in the normal position of the optic disc and fovea are also proposed[40-41]. Multiple factors contribute to the variations in disc-foveal distance, including pathological conditions, and other parameters of the normal population, such as axial length, age, race, myopia status, and glaucomatous conditions[39-41]. Therefore, it should be cautious when using disc-fovea distance to estimate or investigate macular conditions. In summary, we suggest that the LocBscan-3D prediction model should be the primary approach, with the LocEN-2D model serving as an alternative option.

Our study has some limitations. First, the LocBscan-3D model is only reliable and applicable when the fovea has a normal contour and the macula is flat. It may face challenges in detecting the fovea in pathological conditions such as posterior staphyloma, chorioretinal coloboma, and macula pucker. Second, although we considered several previous studies to define the fovea location based on relative distance from the optic disc in the LocEN-2D model, fovea location may not be precisely determined particularly in populations with high myopia. This could be related to factors such as differences in axial length, refractive status, racial differences, and other systemic conditions. Our study used enhanced depth imaging OCT scans with as many as 97 slices. Whereas in real-world practice, fewer slices may be obtained in macula OCT scans and the scanning area may be shallower. Such factors limit the robustness and comprehensiveness of the LocBscan-3D model. While the LocBscan-3D model may not accurately predict

certain macular pathologies, its value remains significant given the predominance of normal foveal contours within the general population. Our model holds potential for practical application in population screening, primarily due to the high prevalence of normal foveal contours. Additionally, the model could operate based on exclusion criteria, which include: 1) failure of the LocBscan-3D model to predict the fovea, 2) significant discrepancy in fovea location between the LocEN-2D and LocBscan-3D models, 3) prediction of SFCT outside the normal range. Under these circumstances, if macular pathologies such as macular pucker or edema are present, leading to inaccurate or failed predictions by the 3D model, such cases can be selectively identified for cautious review or detailed examination. Moreover, previous studies have demonstrated that in the early stages of hypertension or diabetes mellitus, choroidal thickness is thinner compared to the normal population, even in the absence of clinically detectable maculopathy or preclinical retinopathy[31-33]. By detecting subtle abnormalities in SFCT in patients with an otherwise grossly normal macula, early management or further investigation can be initiated. In addition, it would be intriguing to investigate the relationship between B-scan OCT image sequence and en-face OCT or fundus images, as the relative location of the fovea to the optic disc may differ depending on factors such as axial length, refractive error, age, and ethnicity. By applying LocBscan-3D model for fovea detection and combining with en-face OCT image analysis, new reliable rules for the relative position of the optic disc and fovea under various conditions could potentially be established.

In conclusion, our LocBscan-3D model demonstrated accurate prediction of the foveal location, while the LocEN-2D model can serve as an alternative when the LocBscan-3D model fails to detect the fovea. The Mask R-CNN model also provided precise estimations of the SFCT. In order to achieve further enhancement, we look forward to investigations in the future aimed at 1) addressing fovea prediction on pathologic macula without normal contour, 2) determining the valid rules for the relative distance between the optic disc and fovea under different conditions, 3) applying in general population screening.

REFERENCES

1 Ferrara M, Lugano G, Sandinha MT, Kearns VR, Geraghty B, Steel DHW. Biomechanical properties of retina and choroid: a comprehensive review of techniques and translational relevance. *Eye (Lond)* 2021;35:1818-1832.

2 Brinks J, van Dijk EHC, Klaassen I, Schlingemann RO, Kielbasa SM, Emri E, Quax PHA, Bergen AA, Meijer OC, Boon CJF. Exploring the choroidal vascular labyrinth and its molecular and structural roles in health and disease. *Prog Retin Eye Res* 2022;87:100994.

3 Wei WB, Xu L, Jonas JB, Shao L, Du KF, Wang S, Chen CX, Xu J, Wang YX, Zhou JQ, You QS. Subfoveal choroidal thickness: the Beijing eye study. *Ophthalmology* 2013;120(1):175-180.

4 Xie JM, Ye LY, Chen QY, Shi Y, Hu GY, Yin Y, Zou HD, Zhu JF, Fan Y, He JN, Xu X. Choroidal thickness and its association with age, axial length, and refractive error in Chinese adults. *Invest Ophthalmol Vis Sci* 2022;63(2):34.

5 Lin CY, Huang YL, Hsia WP, Wang Y, Chang CJ. Correlation of choroidal thickness with age in healthy subjects: automatic detection and segmentation using a deep learning model. *Int Ophthalmol* 2022;42(10):3061-3070.

6 Entezari M, Karimi S, Ramezani A, Nikkhah H, Fekri Y, Kheiri B. Choroidal thickness in healthy subjects. *J Ophthalmic Vis Res* 2018;13(1):39-43.

7 Lee WK, Baek J, Dansingani KK, Lee JH, Freund KB. Choroidal morphology in eyes with polypoidal choroidal vasculopathy and normal or subnormal subfoveal choroidal thickness. *Retina* 2016;36(Suppl 1):S73-S82.

8 Keenan TD, Klein B, Agrón E, Chew EY, Cukras CA, Wong WT. Choroidal thickness and vascularity vary with disease severity and subretinal drusenoid deposit presence in nonadvanced age-related macular degeneration. *Retina* 2020;40(4):632-642.

9 Liu R, Xuan M, Wang DC, *et al*. Using choroidal thickness to detect myopic macular degeneration. *Int J Ophthalmol* 2024;17(2):317-323.

10 Geraci G, Maria Zammuto M, Vadalà M, *et al*. Choroidal thickness is associated with renal hemodynamics in essential hypertension. *J Clin Hypertens* 2020;22(2):245-253.

11 Masala A, Mola ID, Cellerino M, Pera V, Vagge A, Uccelli A, Christian C, Traverso CE, Iester M. Choroidal thickness in multiple sclerosis: an optical coherence tomography study. *J Clin Neurol* 2022;18(3):334-342.

12 Palma F, Camacho P. The role of Optical Coherence Tomography Angiography to detect early microvascular changes in diabetic retinopathy: a systematic review. *J Diabetes Metab Disord* 2021;20(2):1957-1974.

13 Agra CLDM, Lira RPC, Pinheiro FG, Sá LHSE, Bravo Filho VTF. Optical coherence tomography angiography: microvascular alterations in diabetic eyes without diabetic retinopathy. *Arq Bras Oftalmol* 2021;84(2):149-157.

14 Branchini L, Regatieri CV, Flores-Moreno I, Baumann B, Fujimoto JG, Duker JS. Reproducibility of choroidal thickness measurements

across three spectral domain optical coherence tomography systems. *Ophthalmology* 2012;119(1):119-123.

15 Wakatsuki Y, Shinojima A, Kawamura A, Yuzawa M. Correlation of aging and segmental choroidal thickness measurement using swept source optical coherence tomography in healthy eyes. *PLoS One* 2015;10(12):e0144156.

16 Brown JS, Flitcroft DI, Ying GS, Francis EL, Schmid GF, Quinn GE, Stone RA. *In vivo* human choroidal thickness measurements: evidence for diurnal fluctuations. *Invest Ophthalmol Vis Sci* 2009;50(1):5-12.

17 Hwang S, Kong MG, Song YM, Ham DI. Choroidal spatial distribution indexes as novel parameters for topographic features of the choroid. *Sci Rep* 2020;10(1):574.

18 Hirata M, Tsujikawa A, Matsumoto A, Hangai M, Ooto S, Yamashiro K, Akiba M, Yoshimura N. Macular choroidal thickness and volume in normal subjects measured by swept-source optical coherence tomography. *Invest Ophthalmol Vis Sci* 2011;52(8):4971-4978.

19 Ouyang Y, Heussen FM, Mokwa N, Walsh AC, Durbin MK, Keane PA, Sanchez PJ, Ruiz-Garcia H, Sadda SR. Spatial distribution of posterior pole choroidal thickness by spectral domain optical coherence tomography. *Invest Ophthalmol Vis Sci* 2011;52(9):7019-7026.

20 Yeung SC, You YY, Howe KL, Yan P. Choroidal thickness in patients with cardiovascular disease: a review. *Surv Ophthalmol* 2020;65(4):473-486.

21 Li MH, Zhou J, Chen QY, Zou HD, He JN, Zhu JF, Chen XJ, Shi F, Fan Y, Xu X. Choroid automatic segmentation and thickness quantification on swept-source optical coherence tomography images of highly myopic patients. *Ann Transl Med* 2022;10(11):620.

22 Yan QF, Gu YY, Zhao JY, Wu WJ, Ma YH, Liu J, Zhang J, Zhao YT. Automatic choroid layer segmentation in OCT images *via* context efficient adaptive network. *Appl Intell* 2023;53(5):5554-5566.

23 Masood S, Fang RG, Li P, Li HT, Sheng B, Mathavan A, Wang XN, Yang P, Wu Q, Qin J, Jia WP. Automatic choroid layer segmentation from optical coherence tomography images using deep learning. *Sci Rep* 2019;9(1):3058.

24 Hsia WP, Tse SL, Chang CJ, Huang YL. Automatic segmentation of choroid layer using deep learning on spectral domain optical coherence tomography. *Appl Sci* 2021;11(12):5488.

25 Chen HJ, Huang YL, Tse SL, Hsia WP, Hsiao CH, Wang Y, Chang CJ. Application of artificial intelligence and deep learning for choroid segmentation in myopia. *Transl Vis Sci Technol* 2022;11(2):38.

26 Rothenbuehler SP, Malmqvist L, Belmouhand M, Bjerager J, Maloca PM, Larsen M, Hamann S. Comparison of spectral-domain OCT versus swept-source OCT for the detection of deep optic disc drusen. *Diagnostics* 2022;12(10):2515.

27 2020-2021 BCSC Basic and Clinical Science Course™. Accessed on April 12, 2023. https://www.aao.org/education/bcscsnippetdetail. aspx?id=4df98dde-baa2-4cef-9e19-2b4bc71f604c

28 Williams TD, Wilkinson JM. Position of the fovea centralis with respect to the optic nerve head. *Optom Vis Sci* 1992;69(5):369-377.

29 Rohrschneider K. Determination of the location of the fovea on the fundus. *Invest Ophthalmol Vis Sci* 2004;45(9):3257-3258.

30 Pierro L, Iuliano L, Cicinelli MV, Casalino G, Bandello F. Retinal neurovascular changes appear earlier in type 2 diabetic patients. *Eur J Ophthalmol* 2017;27(3):346-351.

31 Endo H, Kase S, Saito M, Yokoi M, Takahashi M, Ishida S, Kase M. Choroidal thickness in diabetic patients without diabetic retinopathy: a meta-analysis. *Am J Ophthalmol* 2020;218:68-77.

32 Waghamare SR, Mittal S, Pathania M, Samanta R, Kumawat D, Gupta N, Mittal SK. Comparison of choroidal thickness in systemic hypertensive subjects with healthy individuals by spectral domain optical coherence tomography. *Indian J Ophthalmol* 2021;69(5):1183-1188.

33 Papathanasiou KA, Kazantzis D, Vrachatis DA, *et al.* Choroidal thickness in patients with systemic arterial hypertension: a systematic review and meta-analysis. *Ther Adv Ophthalmol* 2022;14: 25158414221132825.

34 Liefers B, Venhuizen FG, Theelen T, Hoyng C, van Ginneken B, Sánchez CI. Fovea detection in optical coherence tomography using convolutional neural networks *Medical Imaging 2017: Image Processing*. Orlando, Florida, USA. SPIE, 2017:19-24.

35 Hussain MS, Deepaisarn S, Aimmanee P. ILM and fovea detection using standard deviation profiling method. *2021 18th International Joint Conference on Computer Science and Software Engineering (JCSSE)*. June 30-July 2, 2021, Lampang, Thailand. IEEE, 2021:1-6.

36 Xu JJ, Zhou Y, Wei QJ, Li K, Li ZP, Yu T, Zhao JC, Ding DY, Li XR, Wang GZ, Dai H. Three-dimensional diabetic macular edema thickness maps based on fluid segmentation and fovea detection using deep learning. *Int J Ophthalmol* 2022;15(3):495-501.

37 Huang HL, Wang GH, Niu LL, Sun XH. Three-dimensional choroidal vascularity index and choroidal thickness in fellow eyes of acute and chronic primary angle-closure using swept-source optical coherence tomography. *Int J Ophthalmol* 2024;17(1):42-52.

38 Orth DH, Fine BS, Fagman W, Quirk TC. Clarification of foveomacular nomenclature and grid for quantitation of macular disorders. *Trans Sect Ophthalmol Am Acad Ophthalmol Otolaryngol* 1977;83(3 Pt 1):OP506-OP514.

39 Dersch A, Hajrasouliha A. Relationship between the disc-fovea distance and axial length. *Investig Ophthalmol Vis Sci* 2020;61(9):PB0011.

40 Girkin CA, McGwin G Jr, Sinai MJ, *et al*. Variation in optic nerve and macular structure with age and race with spectral-domain optical coherence tomography. *Ophthalmology* 2011;118(12):2403-2408.

41 Choi JA, Kim JS, Park HY, Park H, Park CK. The foveal position relative to the optic disc and the retinal nerve fiber layer thickness profile in myopia. *Invest Ophthalmol Vis Sci* 2014;55(3):1419-1426.